ELSEVIER

Int. J. Therm. Sci. 41 (2002) 428–439

International Journal of Thermal Sciences

www.elsevier.com/locate/ijts

Solution of a stationary benchmark problem for natural convection with large temperature difference

Roland Becker, Malte Braack *

Institut für Angewandte Mathematik, Universität Heidelberg, INF 294, 69120 Heidelberg, Germany

Received 2 May 2001; accepted 4 September 2001

Abstract

Computation of compressible flows at low Mach number is often performed by modifications of compressible flow solvers to the low Mach number limit. In particular, time stepping schemes are used where a Poisson problem is solved for pressure updates. In this paper, we propose a different approach for fast computation of stationary solutions. The discretization is made by bilinear and biquadratic finite elements with an elaborated stabilization. It allows the analytical construction of the Jacobian for the whole coupled system. It is used in Newton iterations for solving the nonlinear problems. No time stepping is needed for a wide class of stationary problems. Numerical computations of a benchmark problem for natural convection show the accuracy of the presented method. Different kinds of discretization are compared quantitatively.

Furthermore, the aspect of local mesh refinement is addressed. The local refinement is controled by measuring the discretization error of the sought quantity by *a posteriori* error estimates. This concept is based on solving an adjoint problem which enters in the error estimator as weighting factors of local residuals.

Keywords: Natural convection; Finite elements; Adaptivity; A posteriori error estimates

1. Introduction

In several problems arising in applications, a compressible flow at low Mach number is considered, for instance in free convection, laminar flames etc. In this case, the compression is due to thermodynamical changes and not caused by hydrodynamics. This leads to numerical problems when a purely 'compressible solver' is applied to this type of problems, because they usually determine the pressure by an algebraic equation. Therefore, several papers deal with extensions of compressible flow solvers to hydrodynamically incompressible flows Choi and Merkle [1], or extensions of incompressible schemes to compressible flows Wesseling et al. [2,3] Issa [4] Sampaio and Moreira [5]. In the low Mach number limit, the density is decoupled from the hydrodynamical pressure.

In this paper we develop an efficient numerical method for solving stationary compressible flows with high accuracy. The solver is validated by a benchmark problem recently proposed by Le Quere and Paillere [6] for a heat-driven compressible flow with high temperature difference. It is designed for measuring accuracy and performance of solvers. More than twenty academical groups from Europe and the US participated as well as two commercial CFD companies. The discretization we are going to present, turned out to be one of the most accurate in this benchmark: only two other groups have submitted results with comparable accuracy [6,7]. Since our approach is based on low-order finite elements (at most quadratic), multigrid methods can be used as efficient linear solver. The framework has been already generalized to more complex equations, for instance to combustion problems, see [8–10].

The equations describing flow of a fluid at low Mach number read as follows:

$$\frac{\partial \rho}{\partial t} + \nabla \cdot (\rho v) = 0 \tag{1}$$

$$\frac{\partial (\rho v)}{\partial t} + \nabla \cdot (\rho v \otimes v) + \nabla \cdot \tau + \nabla p - \rho g = -\rho_0 g \tag{2}$$

$$\frac{\partial (\rho T)}{\partial t} + \nabla \cdot (\rho v T) - \nabla \cdot (\kappa \nabla T) = f_{\mathrm{T}} \tag{3}$$

$$\rho = \frac{P_{\mathrm{th}}}{RT} \tag{4}$$

* Correspondence and reprints.

E-mail addresses: roland.becker@iwr.uni-heidelberg.de (R. Becker), malte.braack@iwr.uni-heidelberg.de (M. Braack).

1290-0729/02/$ – see front matter
PII: S1290-0729(02)01335-2

Nomenclature

All dimensional quantities are in SI units.

f_T	source term in the equation for temperature
g	gravitational force
h	mesh-size parameter
H^r	Sobolev space of degree r
I	identity matrix
J	functional
$\langle Nu\rangle_c$	Nusselt number at the cold wall
$\langle Nu\rangle_h$	Nusselt number at the hot wall
p	hydrodynamic pressure
p_{hs}	hydrostatic pressure
P_{th}	thermodynamic pressure
p_{tot}	total pressure
Pr	Prandtl number
R	gas constant
Ra	Raleight number
T	temperature
T_0	$= (T_h + T_c)/2$
T_c	temperature at the cold wall
T_h	temperature at the hot wall
u	$= (p, v, T)$ solution vector
u_h	$= (p_h, v_h, T_h)$ discrete solution vector
v	velocity
x	coordinate

Greek symbols

β	convection
$\delta_p, \delta_v, \delta_T$	stabilization parameters
ε	relative temperature difference
Γ_{out}	outflow part of the boundary
κ	thermal conductivity
μ	viscosity
μ_0	$= \mu(T_0)$ viscosity at temperature T_0
μ^*	reference viscosity
Ω	computational domain
ρ	density
ρ_0	reference density
τ	stress tensor
ξ, ψ, ϕ	test functions

The velocity is denoted by v, temperature by T, density by ρ. The total pressure p_{tot} is split into three parts,

$$p_{tot}(x,t) = P_{th}(t) + p_{hs}(x) + p(x,t)$$

The hydrodynamic pressure is simply denoted by p. The hydrostatic pressure p_{hs} is given by gravitation g and a reference density ρ_0,

$$p_{hs}(x) = \rho_0 \langle g, x\rangle$$

where $\langle g, x\rangle$ denotes the scalar product of the vector of gravitation g and the coordinate x. The thermodynamic pressure P_{th} is constant in space, and in open or unbounded domains also independent of time. The stress tensor τ is given by

$$\tau = -\mu\left\{\nabla v + (\nabla v)^T - \frac{2}{3}(\nabla \cdot v)I\right\}$$

The viscosity μ and the coefficient κ may depend on T. The function f_T denotes a given right-hand side. The system (1)–(4) has to be complemented with appropriate boundary conditions, e.g., Dirichlet, Neumann or Robin conditions.

This system is an approximation of the compressible Navier–Stokes equations, because the hydrodynamic and hydrostatic parts of the pressure are neglected in the equation of state (4) which is justified at low Mach number. This is the case in the problems we consider. As a consequence, the thermodynamic pressure is several magnitudes bigger than $p_{hs} + p$. Due to this simplification, acoustic waves are removed from the system. Recently, a benchmark problem for this kind of flow has been proposed by Le Quere and Paillere [6]. It is designed for investigating accuracy and performance of low-Mach-number solvers. This paper describes this benchmark, illustrates a method for computing this kind of flow and summarizes the obtained results.

The outline of this paper is as follows. We begin in Section 2 with a description of the considered benchmark problem. In Section 3, the discretization of the partial differential equations by stabilized finite elements of equal order for all components is described. Two different formulations are presented. The solution algorithm is presented in the third section. The fourth section deals with the evaluation of output functionals in order to increase the accuracy of the computation. Numerical results of the benchmark problem are given in Section 6, illustrating the performance of the solver and accuracy of the discretizations. We compare the solution obtained with bilinear and biquadratic finite elements. The aspect of adaptivity by local mesh refinement is addressed in Section 7.

The finite element formulation to be presented can be applied to two- and three-dimensional problems in complex geometries. However, for validation, the numerical results presented here deal with a benchmark problem in a simple two-dimensional geometry. In order to emphasize the key features of our approach (finite element formulation, stabilization, and automatic mesh refinement), here, we consider only the stationary setting. The generalization to the far more realistic case of transient flows is the subject of future work.

2. Set up of the benchmark problem

The model consists of a natural convection flow with large temperature differences in a closed cavity $\Omega = [0,1]^2$, see Fig. 1. It is the extension of an earlier comparison (de Vahl Davis and Jones [11]) of flow solvers for incompressible flow using the Boussinesq approximation.

The characteristic model parameters are the Rayleigh number Ra and the non-dimensional temperature difference ε,

$$Ra = Pr\, g\left(\frac{\rho_0}{\mu_0}\right)^2 \cdot \frac{T_\mathrm{h} - T_\mathrm{c}}{T_0}$$

$$\varepsilon = \frac{T_\mathrm{h} - T_\mathrm{c}}{T_\mathrm{h} + T_\mathrm{c}}$$

The quantities $\rho_0 = \rho(T_0, P_0)$ and $\mu_0 = \mu(T_0)$ are density and viscosity at a given reference temperature T_0 and thermodynamic pressure P_0. The parameter ε denotes the relative temperature difference between the hot ($x = 0$) and cold wall ($x = 1$), given by $T_\mathrm{h} = T_0(1+\varepsilon)$ and $T_\mathrm{c} = T_0(1-\varepsilon)$, respectively. At the horizontal (isolated) walls $y = 0$ and $y = 1$, Neumann-type boundary conditions for T are imposed. For the velocities, all boundaries are rigid walls, $v = 0$ on $\partial\Omega$. Fig. 2 shows computed streamlines and isolines of temperature for this benchmark problem.

For the viscosity model, two cases are considered: The Sutherland's law

$$\mu(T) = \mu^*\left(\frac{T}{T^*}\right)^{2/3}\frac{T^* + S}{T + S}$$

and, alternatively, constant viscosity $\mu(T) = \mu(T_0) = \mu_0$. The heat conduction is given in both cases by $\kappa(T) = \mu(T)/Pr$, with constant Prandtl number Pr. The right-hand side f_T in (3) is zero. The exact values of the parameters are given in Table 1.

Furthermore, spatially uniform initial conditions $T = T_0$, and $v = 0$ are imposed for initial time $t = 0$. This leads to an additional unknown in the system: The thermodynamic pressure P_th in a bounded vessel is not any more a given constant but depends on the global temperature distribution, because the initial mass,

$$m_0 = \int_\Omega \rho_0 \,\mathrm{d}x = \frac{P_0}{R}\int_\Omega \frac{1}{T_0}\,\mathrm{d}x$$

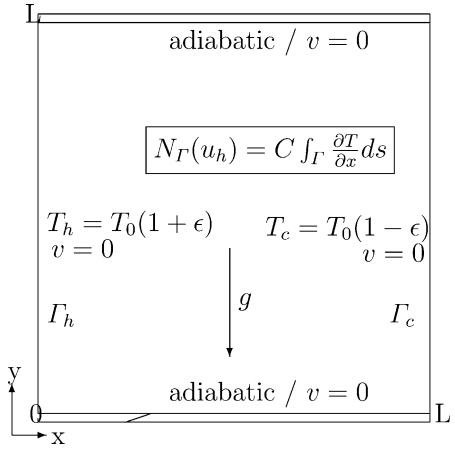

Fig. 1. Configuration of the benchmark problem.

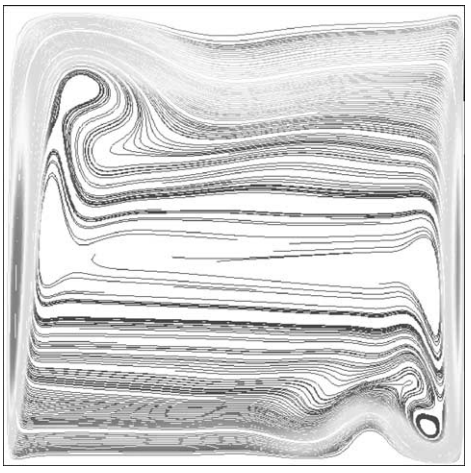

(a)

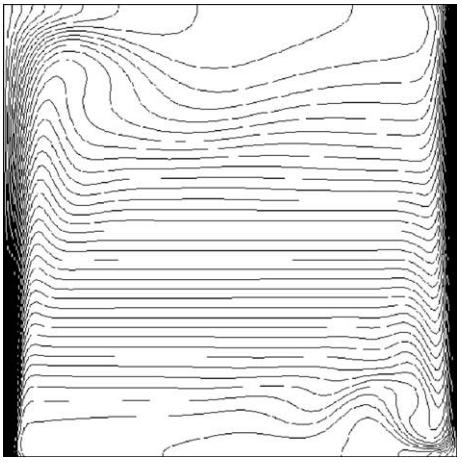

(b)

Fig. 2. Streamlines (a) and isolines of temperature (b) for $Ra = 10^7$.

Table 1
Parameters for the benchmark problem

$T_0 = 600$ K	$T^* = 273$ K	$P_0 = 101325$ Pa	$S = 110.5$ K
$\mu^* = 1.68 \cdot 10^{-5}$ kg·m^{-1}·s^{-1}	$Pr = 0.71$	$\varepsilon = 0.6$	$R = 287$ J·kg^{-1}·K^{-1}

Table 2
Parameters for the test cases

Case	Ra	μ	Reference $\langle Nu\rangle_{\mathrm{h}}$	Values P/P_0
1	10^6	Constant	8.85978	0.856338
2	10^6	Sutherland's law	8.6866	0.9244
3	10^7	Sutherland's law	16.241	0.92263

has to be conserved. Therefore, the thermodynamic pressure for the stationary solution is defined by

$$P_{\mathrm{th}} = P_0\Big(\int_\Omega \frac{1}{T_0}\,\mathrm{d}x\Big)\Big(\int_\Omega \frac{1}{T}\,\mathrm{d}x\Big)^{-1}$$

In this benchmark problem, the quantities of interest are the average Nusselt numbers at the hot and cold walls, Γ_{h} and Γ_{c}, respectively, given by

$$\begin{aligned}\langle Nu\rangle_{\mathrm{h}} &= c\int_{\Gamma_{\mathrm{h}}} \kappa\frac{\partial T}{\partial n}\,\mathrm{d}x \quad \text{and}\\ \langle Nu\rangle_{\mathrm{c}} &= c\int_{\Gamma_{\mathrm{c}}} \kappa\frac{\partial T}{\partial n}\,\mathrm{d}x \qquad (5)\\ c &= \frac{Pr}{\mu_0 T_0 2\varepsilon}\end{aligned}$$

for the unitsquare Ω. The sum of these averages is zero, because of the Neumann-type conditions at the upper and lower wall for T and the non-slip conditions for the velocities,

$$\begin{aligned}\langle Nu\rangle_{\mathrm{h}} + \langle Nu\rangle_{\mathrm{c}} &= c\int_{\partial\Omega}\Big(\kappa\frac{\partial T}{\partial n} - \rho v\cdot n\Big)\,\mathrm{d}x\\ &= c\int_\Omega \big(\rho v\cdot\nabla T - \nabla\cdot(\kappa\nabla T)\big)\,\mathrm{d}x = 0\end{aligned}$$

However, for discrete solutions, one expects an error which should converge to zero under mesh refinement. We will evaluate the relative difference for the discrete solutions, given by

$$\langle e\rangle := 1 + \frac{\langle Nu\rangle_{\mathrm{c}}}{\langle Nu\rangle_{\mathrm{h}}}$$

Three test case of increasing difficulty are considered as listed in Table 2. Moreover, the reference solution [7] determined by the organizers of the benchmark is given. In case 3, the strongest boundary layers for temperature and velocities occur. This configuration is very close to the non-stationary limit. Therefore, solving such problems with a pure stationary solver is not an easy task. Normally, time stepping is performed using several hundreds or even thousands of time steps. Due to the discretization and the fully coupled implicit solution process, presented later, we are able to solve such problems by a few nonlinear iteration steps.

3. Discretization

We begin by setting the frame for a Galerkin finite element discretization. For notational simplicity, we consider the case that the computational domain $\Omega\subset\mathbb{R}^d$ is polygonal ($d=2$) or polyhedral in 3D ($d=3$). Extensions for curved boundaries are possible. By $L^2(\Omega)$, we denote the Lebesgue space of square-integrable functions on Ω, equipped with the inner product and norm

$$\begin{aligned}(f,g) &:= \int_\Omega f(x)g(x)\,\mathrm{d}x\\ \|f\| &:= \Big(\int_\Omega |f(x)|^2\,\mathrm{d}x\Big)^{1/2}\end{aligned}$$

The suggestive notation $(f,g)_Q$ and $\|f\|_Q$ is used for the L^2 inner product and norm on a subset $Q\subset\Omega$.

The variational formulation of (1)–(4) for the unknowns $u=(p,v,T)$ is obtained by multiplying the equations by appropriate test vector functions $\varphi=(\xi,\phi,\psi)$ and integrating over Ω. This leads us to introduce a semi-linear form $a(\cdot,\cdot)$ by

$$\begin{aligned}a(u,\varphi) &:= \big(\nabla\cdot v - T^{-1}v\cdot\nabla T,\xi\big)\\ &\quad + (\rho v\cdot\nabla v,\phi) - (\tau,\nabla\phi) - (p,\nabla\cdot\phi)\\ &\quad - (\rho g,\phi) + (\rho v\cdot\nabla T,\psi) + (\kappa\nabla T,\nabla\psi) \qquad (6)\end{aligned}$$

The test functions φ are elements of the space $X = Q\times V^d\times V$, with $Q=L^2(\Omega)$ and the Sobolev space $V = H_0^1(\Omega)$, i.e., the space of functions with L^2 integrable generalized first derivatives. The weak formulation reads,

$$u\in u_0+X\colon\ a(u,\varphi)=(f,\varphi)\ \forall\varphi\in X \qquad (7)$$

with Dirichlet data u_0 on (or parts of) the boundary $\partial\Omega$. Neumann-type boundary conditions are implicitly represented because of the partial integration of the diffusive terms. Non-homogeneous Dirichlet boundary conditions u_0 have to be explicitly imposed on the solution. The function $f=(0,-\rho_0 g,f_{\mathrm{T}})\in L^2(\Omega)^{2+d}$ is the given right-hand side. The density ρ is considered as a variable coefficient depending on temperature according to (4). The space for the hydrodynamical pressure is $L^2(\Omega)$. If Dirichlet conditions for the velocity are imposed along the entire boundary, the hydrodynamical pressure is only defined modulo a constant and the corresponding pressure space is $L^2(\Omega)/\mathbb{R}$. If an outflow boundary Γ_{out} is present, the partial integration of the pressure gradient imposes implicitly the 'natural' outflow condition

$$-\mu\frac{\partial v}{\partial n} + pn = 0 \quad \text{on } \Gamma_{\mathrm{out}}$$

On a discussion on this boundary condition, we refer to Heywood, et al. [12]. However, in the benchmark configuration presented above, no outflow condition is necessary.

Another possibility is a 'conservative formulation' where the convective fluxes are partially integrated. Instead of (6), one may consider the semi-linear form $b(\cdot,\cdot)$ given by

$$
\begin{aligned}
b(u,\varphi) :=\ & -(\rho v, \nabla\xi) - (\rho v \otimes v + \tau, \nabla\phi) \\
& - (p, \nabla\cdot\phi) - (\rho g, \phi) \\
& - C(v, \nabla\psi) + (\kappa \nabla T, \nabla\psi) \\
& + \int_{\partial\Omega} \rho v \cdot n\, \xi \,\mathrm{d}x + \int_{\partial\Omega} (\rho v \otimes v)\cdot n \phi \,\mathrm{d}x \\
& + C \int_{\partial\Omega} v \cdot n \psi \,\mathrm{d}x
\end{aligned} \tag{8}
$$

with the constant $C := P_{\mathrm{th}}/R$. The arising boundary integrals vanish if homogeneous Dirichlet conditions for the velocities are imposed on the whole boundary (closed vessel), as in the benchmark problem described above. In this formulation, no convective term arises in the equation for the temperature.

Our discretization uses a conforming Galerkin finite element method defined on quadrilateral (or hexahedral) meshes $\mathcal{T}_h = \{K\}$ on $\Omega \subset \mathbb{R}^d$, with cells denoted by K. The trial and test spaces $X_h \subset X$ consist of continuous, piecewise polynomial vector functions (so-called Q_r-elements) for all unknowns,

$$X_h = \left\{\varphi_h \in C\left(\overline{\Omega}\right); \varphi_h|_K \in (Q_r)^{2+d}\right\}$$

where Q_r is the space of (isoparametric) d-linear ($r = 1$) or d-quadratic ($r = 2$) polynomials in d space dimensions obtained by transformations of a fixed reference unit cell $\widehat{K}$. For a detailed description of this standard construction, see Ciarlet [13] or Johnson [14].

Eq. (7) includes as a special case the linear Stokes system, the discretization of which requires a certain stability condition (so-called Babuska–Brezzi condition [15]) to be satisfied. It is well-known that the use of equal-order elements for velocity and pressure is ruled out in the standard Galerkin formulation. This limitation can be overcome for instance by least-squares stabilization. Instead of directly discretizing equation (7), we introduce a stabilization term which depends on the mesh-size h. The stabilization has to serve several purposes, the treatment of the stiff pressure-velocity coupling in the low-Mach number approximation, the stabilization of the advective terms, and finally the enhancement of local mass conservation. The modification is done in a consistent way, i.e., the solution of the partial differential equation representing (1)–(4) satisfies also these stabilized equations.

For the presentation of our stabilization, we write the considered system (1)–(4) of PDEs in operator form,

$$
\begin{aligned}
& Lu = f \quad \text{in } \Omega \\
& u = u_0 \quad \text{on } \partial\Omega
\end{aligned}
$$

Following ideas of Hughes et al. [16] for the (incompressible) Navier–Stokes equations, the stabilization is accomplished by introducing additional least-squares terms in the continuity equation. We use a variant of this technique: The discrete semi-linear form we consider is defined by use of a stabilization operator S specified below,

$$a_h(u,\varphi) := a(u,\varphi) + \langle Lu, S\varphi\rangle_\delta \tag{9}$$

For simplifying notation, we use here the mesh-dependent L^2 inner product for scalar functions

$$\langle u, v\rangle_\delta := \sum_{K\in\mathcal{T}_h} \delta_K (u,v)_K$$

with dependent vector-valued weights δ_K depending on u. The discretization of (7) is of the form

$$u_h \in X_h\colon\ a_h(u_h,\varphi) = (f,\varphi) + \langle f, S\varphi\rangle_\delta \ \forall \varphi \in X_h \tag{10}$$

The operator S is chosen as follows. We split the Frechét derivative of L in the differential part P and a part Z consisting of zero-order terms:

$$L'[u] = P + Z$$

Whereas in Galerkin least-squares techniques, the stabilization is chosen as $P + Z$, we choose the stabilizaton operator as the negative adjoint: $S = -P^*$. Using the fact that ρv is solenoidal, this choice leads to the following operator S:

$$S = -P^* = \begin{bmatrix} 0 & \mathrm{div} & 0 \\ \nabla & \beta\cdot\nabla + \nabla\cdot\mu\nabla & 0 \\ \alpha\cdot\nabla & 0 & \beta\cdot\nabla + \nabla\cdot\kappa\nabla \end{bmatrix}$$

with $\beta = \rho v$ and $\alpha = -T^{-1}v$. Since S does not contain zero-order terms, the stabilization term vanishes on constants. This is an important feature for a global conservation property of the semi-linear form $b_h(\cdot,\cdot)$, as pointed out in detail in Section 5. Note, that the stabilization operator S is the same for both semi-linear forms a_h and b_h, since its definition is only based on the partial differential operator L.

By elementary calculus, this setting yields the following stabilization terms:

$$
\begin{aligned}
& \langle Lu, S\varphi\rangle_\delta \\
& \quad = \sum_K \big\{ \delta_p(\nabla\cdot v - \alpha\cdot\nabla T, \nabla\cdot\phi) && (11) \\
& \qquad + \delta_v\big(\beta\cdot\nabla v - \nabla\cdot(\mu\nabla v) + \nabla p - \rho g, \nabla\xi\big) && (12) \\
& \qquad + \delta_v\big(\rho v\cdot\nabla v - \nabla\cdot(\mu\nabla v) + \nabla p - \rho g, \\
& \qquad\quad \beta\cdot\nabla\phi + \nabla\cdot(\mu\nabla\phi)\big) && (13) \\
& \qquad + \delta_T\big(\beta\cdot\nabla T - \nabla\cdot(\kappa\nabla T), \\
& \qquad\quad \beta\cdot\nabla\psi + \nabla\cdot(\kappa\nabla\psi)\big) && (14) \\
& \qquad + \delta_T\big(\beta\cdot\nabla T - \nabla\cdot(\kappa\nabla T), \alpha\cdot\nabla\xi\big)\big\} && (15)
\end{aligned}
$$

We will discuss several of the terms arising above in order to clarify this setting. The term (12) accomplished the pressure-velocity stabilization according to [16]. Here, the essential part for stabilization is $\langle\nabla p, \nabla\xi\rangle_\delta$ acting like a Laplacian on the pressure. The other terms in (12) are needed for consistency: They vanish for the exact solution u of (1)–(4). The term (13) includes stabilization of the convective term in the momentum equation by streamline diffusion [14]. Here, the essential part is $\langle\beta\cdot\nabla v, \beta\cdot\nabla\phi\rangle_\delta$. The convective part

in the equation for temperature is stabilized in the same way by the term $\langle \beta \cdot \nabla T, \beta \cdot \nabla \psi \rangle_\delta$ in (14). Hansbo and Szepessy proposed in [17] for the (incompressible) Navier–Stokes equations a further stabilization term $\langle \nabla \cdot v, \nabla \cdot \phi \rangle_\delta$, in order to enforce mass conservation. Generalization to compressible flows is obtained by the term in (11). The convective part in the continuity equation due to density variations is stabilized by $\langle \beta \cdot \nabla T, \alpha \cdot \nabla \xi \rangle_\delta$ in (15). The stabilization parameters $\delta_K = \delta_0 \cdot \mathrm{diag}\{\delta_p, \delta_v, \delta_T\}$ form a diagonal matrix. They are chosen cell-wise, depending on the balance between local convection $\beta_K = |\rho v|_{K,\infty}$ and the diffusion parameters μ and κ, according to

$$\delta_p = \beta_K^2 \delta_v$$

$$\delta_v = \frac{h_K^2}{c\mu + \beta_K h_K}$$

$$\delta_T = \frac{h_K^2}{c\kappa + \beta_K h_K}$$

The choice of the constant δ_0 should depend on the order of the discretization. For Q_1 elements, $0.2 \leqslant \delta_0 \leqslant 0.5$ is appropriate, but δ_0 can be chosen smaller for higher-order elements. Further, we set $c = 12$ for Q_1, and $c = 50$ for Q_2 elements, according to Franca and Frey [18].

4. Solver

Many approaches for computing low-Mach-number flow are based on time-stepping and splitting techniques. In those methods, each time step is splitted in several substeps, where sucessive velocity and pressure updates are performed. Usually, at least one Poisson problem has to be solved in order to get the pressure update. While each time step in splitting methodes may be relatively cheap, they often suffer when the nonlinearity becomes more important. Then, many time steps are needed for reaching a stationary solution.

Therefore, we propose a different approach. The whole system is solved in a fully coupled and implicit manner by a Newton-type method. The approximate Jacobian is derived from an analytical derivative of the variational system (10), for simplicity neglecting the u-dependence in the stabilization parameters δ_K. Furthermore, also the variation of the coefficients μ and κ is neglected in the Jacobian. This means, that these parameters are frozen at the current discrete solution u_h, while the derivatives $\partial\mu/\partial T$ and $\partial\kappa/\partial T$ are assumed to be small.

Each iteration step requires the solution of a linear system which represents the discretization of a linear partial differential equation. Even in the case of mere diffusion expressed by the Laplacian operator, which is always part of our system, the inversion by a direct solver or by a simple iterative scheme like the Conjugated Gradient Method (CG) is prohibitive due to increasingly bad conditioning of the algebraic system under mesh refinement. We use the Generalized Minimal Residual Method (GMRES), see Saad [19], with preconditioning by a multigrid iteration organized as a V-cycle, see Hackbusch [20]. The GMRES method is specially suitable for non-symmetric and indefinite matrices. The use of a multigrid preconditioner makes the relevant condition number independent of the number of grid points which is especially important on locally refined meshes.

The meshes used in our computations have cells with 'hanging nodes' to facilitate local refinement and coarsening, see Fig. 3. The unknowns corresponding to such irregular nodes are eliminated from the system. For the evaluation of integrals on the mesh cells the 4-point Gauss formula is used. The design of multigrid algorithms on such meshes requires some care. While the highest level consists of all unknows, the lower levels are obtained recursively by a global coarsening technique. For details of the implementation and comparisons to other multigrid techniques we refer to [21]. For smoothing, a defect correction iteration is used based on block-ILU decomposition on each level of the hierarchical mesh. The linear equations are solved up to a tolerance determined by the convergence rate of the nonlinear residual. Strategies for specifying appropriate tolerances have been proposed by Kelley in [22]. The full algorithm is described in detail in [10].

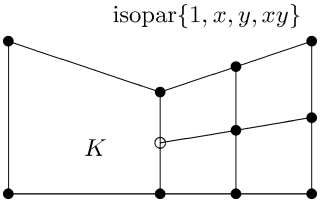

Fig. 3. Quadrilateral mesh in 2D with 'hanging node'.

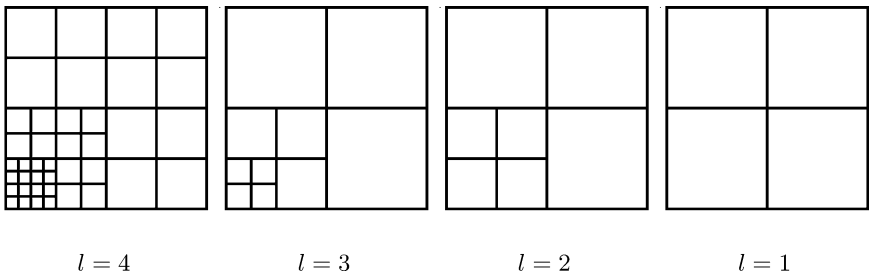

Fig. 4. Sequence of meshes for the multigrid solver.

5. Evaluation of boundary functionals

In this section, we discuss the numerical evaluation of the averaged Nusselt number

$$J(u) = \int_{\Gamma} \kappa \frac{\partial T}{\partial n} \,\mathrm{d}s \tag{16}$$

over a part of the boundary $\Gamma \subset \partial\Omega$. In principle, the boundary integral (16) could be evaluated exactly for the discrete temperature T_h since it is a finite element function. This method would be for piecewise bilinear elements only of first order. Therefore, we present a more precise computation which is for bilinear finite elements of second order. We refer to Giles et al. [23] and the literature therein for a similar technique for the computation of the drag coefficient of an incompressible flow.

We denote by $\Gamma_D \subset \partial\Omega$ that part of the boundary, where Dirichlet conditions for T are imposed. We chose a test function $z = (0, 0, \psi)$ where $\psi = 1$ on $\Gamma \cap \Gamma_D$ and $\psi = 0$ on $\Gamma_D \setminus (\Gamma \cap \Gamma_D)$. Notice that $z \notin X$. Since u is the solution of the continuous problem, the residual respect to z turns out to be

$$\begin{aligned} &a(u,z) - (f,z) \\ &\quad = (\rho v \cdot \nabla T, \psi) + (\kappa \nabla T, \nabla \psi) - (f_\mathrm{T}, \psi) \\ &\quad = \big(\rho v \cdot \nabla T - \nabla \cdot (\kappa \nabla T) - f_\mathrm{T}, \psi\big) + \int_{\Gamma} \kappa \frac{\partial T}{\partial n} \psi \,\mathrm{d}s \\ &\quad = J(u) \end{aligned}$$

Therefore, we obtain the alternative presentation

$$J(u) = a(u,z) - (f,z) \tag{17}$$

for an arbitrary test function z with setting on the boundary as described above. Analogous, we define the functional J_h for discrete solutions u_h by use of the semi-linear form a_h,

$$J_h(u_h) := a_h(u_h, z_h) - (f, z_h) - \langle f, S z_h \rangle_\delta \tag{18}$$

where the discrete z_h has the same boundary value as z. This means from the practical point of view, that evaluation of $J_h(u_h)$ can be realized by only one residual evaluation with an appropriate test function z_h. This definition of $J_h(u_h)$ does not depend on the specific choice of z_h, since for two discrete test functions $z_h^i = (0, 0, \psi^i)$, $i = 1, 2$, with $\psi^1 = \psi^2 = 1$ on $\Gamma \cap \Gamma_D$, and $\psi^1 = \psi^2 = 0$ on $\partial\Omega \setminus (\Gamma \cap \Gamma_D)$, there holds $\phi := z_h^1 - z_h^2 \in X_h$. As a consequence, ϕ can be inserted in (10).

In the case of homogeneous boundary conditions for the velocities and $\Gamma = \Gamma_D$, the functional (16) can be written as a integral of the right-hand side f_T as follows: We may choose $\psi \equiv 1$ and obtain

$$\begin{aligned} J(u) &= (\rho v \cdot \nabla T - f_\mathrm{T}, \psi) \\ &= \int_{\delta\Omega} \rho v \cdot n T \,\mathrm{d}x - \int_{\Omega} f_\mathrm{T} \,\mathrm{d}x = -\int_{\Omega} f_\mathrm{T} \,\mathrm{d}x \end{aligned}$$

This reflects the energy conservation in the system. For the practical evaluation of (18), one chooses the constant test function $z_h = (0, 0, 1)$ on Ω. The stabilization term $S z_h$ vanishes in this case, since it involves only derivatives of z_h. We apply this way of functional evaluation to the two stabilized semi-linear forms a_h and b_h described in the previous section, and denote the resulting quantities by J_a and J_b, respecively. There holds

$$\begin{aligned} J_b(u_h) &= b(u_h, z_h) = -\int_{\Omega} f_\mathrm{T} \,\mathrm{d}x = J(u) \\ J_a(u_h) &= a(u_h, z_h) = \int_{\Omega} (\rho v_h \cdot \nabla T_\mathrm{h} - f_\mathrm{T}) \,\mathrm{d}x \\ &= J(u) + \int_{\Omega} \rho v_h \cdot \nabla T_\mathrm{h} \,\mathrm{d}x \end{aligned}$$

From these identities, we deduce that the scheme based on (8) conserves the global Nusselt number, while the use of the semi-linear form a_h lacks such a property. The numerical results presented later will confirm this result.

An error analysis using a duality argument gives the following estimate

$$\big|J(u) - J_h(u_h)\big| \leqslant \big|a'[u](e, \varepsilon)\big| + R(e)$$

where $e := u - u_h$ denotes the discretization error, $\varepsilon := z - i_h z$ the interpolation error of the solution z of an corresponding dual problem (see Section 7), and $R(e)$ a remainder term of order $\mathrm{O}(e^2)$. The expression $a'[u]$ denotes the Frechét derivative of the semi-linear form $a(\cdot,\cdot)$ at the solution u. For Q_1 elements, sufficiently regular solutions, i.e., $u, z \in H^2(\Omega)$, and an uniform mesh size h, the asymptotic bound for the main part is

$$\big|a'[u](e, \varepsilon)\big| \leqslant C h^2 |u|_2 |z|_2$$

with the H^2 norm $|\cdot|_2$. For quadratic finite elements Q_2, the error $|J(u) - J_h(u_h)|$ will be even of order $\mathrm{O}(h^4)$.

6. Numerical results

Now we report on the results obtained for the benchmark problem presented in Section 2. We investigate three types of discretization using formulations according to (6) and (8) as listed in Table 3. The quantities of interest are the average Nusselt numbers, the relative error and the change of thermodynamic pressure relative to the initial pressure P_0 for the proposed discretizations of the semilinear forms $a(\cdot,\cdot)$ and $b(\cdot,\cdot)$.

Table 3
Three investigated types of discretizations

	Element	Formulation
Discr I	Q_1	Non-conservative $a_h(\cdot,\cdot)$
Discr II	Q_1	Conservative $b_h(\cdot,\cdot)$
Discr III	Q_2	Conservative $b_h(\cdot,\cdot)$

Table 4
Semilinear form $a_h(\cdot,\cdot)$ with Q_1 elements for Case 1

#dof	*Discr I*				*Discr II*	
	$\langle Nu\rangle_h$	$\langle Nu\rangle_c$	$\langle e\rangle$	P/P_0	$\langle Nu\rangle_h$	P/P_0
1 156	9.08551	−8.09644	1.09e−1	0.853062	8.8390848	0.83557155
4 356	9.02496	−8.61103	4.59e−2	0.857608	8.7408160	0.86185000
16 900	8.91595	−8.79795	1.32e−2	0.856444	8.8233059	0.85853977
66 564	8.87970	−8.84576	3.82e−3	0.856270	8.8516398	0.85689606
264 196	8.86590	−8.85667	1.04e−3	0.856298	8.8580892	0.85646566
1 052 676	8.86147	−8.85907	2.72e−4	0.856324	8.8594183	0.85636724
4 202 500	8.86022	−8.85960	6.93e−5	0.856334	8.8596967	0.85634487
extrapolated	8.85979	−8.85979	0	0.856337	8.85978	0.856337

These numerical computations are performed in order to test the discretization on an equidistant tensor mesh. Better values for the Nusselt number can be obtained by adjusting the underlying coarsest mesh in order to resolve the boundary layers more accurately. Furthermore, as addressed in the last section, local mesh refinement will increase the performance (relationsship between error and computational cost #dof) substantially.

6.1. Reference solution for constant coefficients: Case 1

In Table 4, the results for the formulation based on *Discr I* and *Discr II* (Q_1 elements) in dependence of the number of degrees of freedom (#dof) are given. All quantities converge with second order in the mesh size h. However, for *Discr I* there is still the expected gap between $\langle Nu\rangle_h$ and $\langle Nu\rangle_c$ due to the non-conservative formulation. The relative difference behaves like $O(h^2)$. The extrapolated value is obtained on the basis of the solutions of the two finest grids. For the 'conservative formulation' *Discr II* (and *Discr III*), the absolute value of the two averaged Nusselt numbers along the hot and cold wall is the same up to (machine) truncation error 10^{-8}. Therefore, we presented only the results for $\langle Nu\rangle_h$. Comparison between both formulations shows that they converge to the same quantities for the Nusselt numbers and the quotient P/P_0. Beside the fact that *Discr II* conserves the overall Nusselt number, both variants do not show substantial differences.

The organizing commitee determined the Nusselt numbers up to 6 decimals as

$$\langle Nu\rangle_h = -\langle Nu\rangle_c = 8.85978$$

see [6] and [7]. The official reference pressure is $P/P_0 = 0.856337$. Our obtained values in Table 4 agree extremely well with these reference values.

6.2. Reference solution for variable coefficients: Case 2

In the case of variable coefficient given by Sutherland's law, the conservative formulation is also advantageous for determination of the Nusselt number, see Tables 5 and 6. The thermodynamical pressure P is captured with the same accuracy by both formulations. In this case, substantial improved can be obtained by the use of Q_2 elements. It can be seen in Table 6, that the order of the method with polynomials of second order gives accuracy in the Nusselt number of order $O(h^4)$, resulting in a more reliable solution.

Table 5
Semilinear form $a_h(\cdot,\cdot)$ with Q_1 elements for Case 2

#dof	*Discr I*			
	$\langle Nu\rangle_h$	$\langle Nu\rangle_c$	$\langle e\rangle$	P/P_0
1 156	9.33273	−8.21159	1.20e−1	0.900862
4 356	9.21050	−8.33739	9.48e−2	0.931489
16 900	8.87338	−8.58009	3.31e−2	0.927150
66 564	8.74806	−8.65797	1.03e−2	0.925258
264 196	8.70491	−8.67965	2.89e−3	0.924663
1 052 676	8.69161	−8.68495	7.66e−4	0.924524
4 202 500	8.68790	−8.68619	1.96e−4	0.924495
extrapolated	8.68663	−8.68663	0	0.924485

Table 6
Semilinear form $b_h(\cdot,\cdot)$ with Q_1 and Q_2 elements for Case 2

#dof	*Discr II*		*Discr III*	
	$\langle Nu\rangle_h$	P/P_0	$\langle Nu\rangle_h$	P/P_0
4 356	8.5634737	0.92994689	8.5086302	0.93899719
16 900	8.6156824	0.92894797	8.6474278	0.92767292
66 564	8.6655591	0.92590062	8.6820791	0.92488610
264 196	8.6814607	0.92484334	8.6862850	0.92453102
1 052 676	8.6854006	0.92457115	8.6866173	0.92449122
4 202 500	8.6863068	0.92450708	8.6866015	0.92448762
extrapolated	8.6866089	0.92448572	8.6866005	0.92448762

The organizer of the benchmark states the reference value for the Nusselt number up to 5 digits as

$$\langle Nu\rangle_h = 8.6866, \qquad P/P_0 = 0.9244$$

6.3. Reference solution for variable coefficients: Case 3

The results for the most delicate case of Rayleigh number 10^7 are given in Tables 7 and 8. The official reference values are

$$\langle Nu\rangle_h = 16.241, \qquad P/P_0 = 0.92263$$

The performance of the three types of discretization are similar to Case 2: The conservative formulation with Q_2 elements converges with order $O(h^4)$ in the Nusselt number. The pressure is obtained with accuracy of at least $O(h^3)$.

Table 7
Semilinear form $a_h(\cdot,\cdot)$ with Q_1 elements for Case 3

#dof	*Discr I*			
	$\langle Nu\rangle_h$	$\langle Nu\rangle_c$	$\langle e\rangle$	P/P_0
4 356	17.5800	−14.9106	1.52e−1	0.929152
16 900	17.0268	−15.6505	8.08e−2	0.932336
66 564	16.5194	−16.0793	2.66e−2	0.925433
264 196	16.3345	−16.2000	8.14e−3	0.923354
1 052 676	16.2697	−16.2315	2.35e−3	0.922782
4 202 500	16.2491	−16.2389	6.27e−4	0.922661

Table 8
Semilinear form $b_h(\cdot,\cdot)$ with Q_1 and Q_2 elements for Case 3

#dof	*Discr II*		*Discr III*	
	$\langle Nu\rangle_h$	P/P_0	$\langle Nu\rangle_h$	P/P_0
4 356	14.680692	0.95142424	14.773900	0.96438500
16 900	15.916378	0.93352524	15.911297	0.93749682
66 564	16.114378	0.92760636	16.181554	0.92552776
264 196	16.206343	0.92408765	16.234209	0.92300012
1 052 676	16.232851	0.92299167	16.240524	0.92267494
4 202 500	16.239162	0.92271702	16.241026	0.92263807
extrapolated	16.241266	0.92262547	16.241076	0.92263570

6.4. Performance of the solver

In Table 9, we show the convergence rates in the solver for computations on globally refined meshes with *Discr I* (Q_1 elements). The second column includes the convergence rate ϱ of the nonlinear iteration. For a reduction of the residual by the factor of 10^{10}, the number of needed iterations is given in the third column. Furthermore, the number of assembled Jacobians is given. Instead of building the Jacobian in each nonlinear step, it is kept if the reduction of the residual of the previous step is better than a factor of 0.2. The fourth column shows the reduction rate of the linear solve in the last nonlinear step. The average number of linear iterations in each nonlinear step is given in the last column. In each iteration, two pre- and two post-smoothing steps are performed.

Under mesh refinement, the number of Newton steps needed decreases significantly. On the finer meshes between 1 and 4 million unknowns, only one Jacobian is assembled for reducing the residual by 10 digits. This can be observed in all three test cases. The linear convergence benefits also from mesh refinement, leading to reduction rates of about 0.1. On the finest mesh, only two multigrid iterations are necessary for reducing the linear residual by a factor of 0.01. This behavior is due to the fact that the arising matrices become more and more definite, while the multigrid solver is independent of the condition number.

For comparisons, we included in Table 9 the corresponding values for Q_2 elements on a mesh with 263 169 nodes (about 4 million unknowns) for Case 2. In order to achieve similarly robust convergence, we increased the effort in the multigrid cycle to 8 pre- and 8 post-smoothing steps.

Table 9
Convergence record for Q_1 elements (*Discr I*). Columns left to right: degrees of freedom (#dof), nonlinear convergence rate (ϱ), nonlinear iterations, number of used Jacobians, linear convergence rate, linear iterations/nonlinear step

#dof	Nonlinear			Linear	
	ϱ	Iterations	Jacobians	Rate	Iterations
Case 1					
1 156	0.24	14	9	0.303	5.0
4 356	0.17	12	7	0.123	2.8
16 900	0.17	12	7	0.137	2.8
66 564	0.03	6	3	0.100	2.7
264 196	0.01	4	1	0.052	2.0
1 052 676	< 0.01	3	1	0.042	2.3
4 202 500	< 0.01	3	1	0.012	1.7
Case 2					
1 156	0.37	19	17	0.256	5.1
4 356	0.30	16	10	0.182	3.4
16 900	0.23	14	9	0.178	3.2
66 564	0.13	10	3	0.115	2.8
264 196	0.10	8	1	0.073	2.0
1 052 676	0.09	8	1	0.026	2.0
4 202 500	0.07	7	1	0.012	1.8
(Q_2)	0.11	9	4	0.139	3.0
Case 3					
1 156	0.62	20	20	0.383	7.5
4 356	0.21	12	7	0.366	5.2
16 900	0.17	11	2	0.389	4.7
66 564	0.15	10	4	0.166	3.5
264 196	0.10	8	1	0.106	2.6
1 052 676	0.09	8	1	0.036	2.0

The CPU time needed with a Pentium III, 1 GHZ, is with Q_1 elements in Case 2 for computing the stationary solution and evaluating the functionals as follows: for 16 900 degrees of freedom 20 s, for 66 564 dof's 73 s, for 264 196 dof's 200 s and for 1 052 676 dof's 840 s. The other cases show very similar computing times.

7. Adaptive local refinement

Adaptive mesh refinement is well known to be an efficient method to increase the accuracy of the discrete solution with respect to the number of degrees of freedom. In order to facilitate local mesh refinement and coarsening, we allow the cells in the refinement zone to have nodes which lie on faces of neighboring cells, see Fig. 3. But not more than two of such 'hanging nodes' are allowed per cell. The degrees of freedom corresponding to these irregular nodes are eliminated from the system enforcing global conformity (i.e., continuity across inter-element boundaries) for the finite element functions. In the case $r \geqslant 2$, several degrees of freedom on 'hanging edges' have to be eliminated.

The efficiency of local mesh refinement strongly depends on the refinement strategy and the information about discretization errors. The *a posteriori error* estimates based on weighted residuals, introduced by Becker and

Rannacher [24], has already been successfully applied to various kinds of PDEs: Navier–Stokes [25], combustion problems [8,9] and elasto-plasticity [26]. Before applying this technique to the considered benchmark problem, we shortly recall the estimator for the error in the average Nusselt number.

According to (5), the average Nusselt number can be considered as the functional

$$J(u) = c \int_{\Gamma_c} \kappa \frac{\partial T}{\partial n} \, \mathrm{d}x$$

We employ a 'duality argument' as common in the error analysis for finite element Galerkin methods. The functional $J(\cdot)$ (respectively its linearization) is taken as 'forcing term' in a 'dual problem' governed by the linearized adjoint operator L'^*. This operator was already introduced for the definition of the stabilization. The dual problem was already used for the error analysis of the functional evaluation in Section 5. From the solution of this dual problem, we derive the weights which describe the contribution of the local cell-residuals to the error quantity $|J(u) - J(u_h)|$. This information is then used for quantitative error control and as a criterion for local mesh refinement as described before. The whole process may be viewed as a sensitivity analysis of the given continuous model with respect to the perturbations induced by the finite element discretization. The key for the efficiency of the resulting a posteriori error estimates is the so-called 'Galerkin orthogonality' inherent to the finite element approach, i.e., the orthogonality of the variational residual to the discrete test space.

Here, we assume $J(\cdot)$ to be linear, although in the case of the Nusselt number we have a weak nonlinearity if the coefficient κ varies with temperature. However, the whole approach can be extended to nonlinear functionals, see [24]. Using the Galerkin orthogonality of the finite element scheme an error bound of the form

$$\begin{aligned} &\big|J(u) - J(u_h)\big| \\ &\quad \leqslant \eta_\omega := \sum_{K \in \mathcal{T}_h} \big\{ \varrho_K (\omega_K + \omega_{K,\delta}) + \varrho_{\partial K} \omega_{\partial K} \big\} \end{aligned} \tag{19}$$

can be derived, see [8]. This a posteriori error estimator contains cell-residuals

$$\varrho_K := \|f - Lu_h\|_K$$
$$\varrho_{\partial K} := h_K^{-1/2} \big\| \big[\partial_n^L u_h\big] \big\|_{\partial K}$$

and weights

$$\omega_K = \|z - z_h\|_K$$
$$\omega_{K,\delta} = \delta_K \big\| S(z - z_h) \big\|_K$$
$$\omega_{\partial K} = h_K^{-1/2} \|z - z_h\|_{\partial K}$$

The cell residual terms ϱ_K and $\varrho_{\partial K}$ depend only on the discrete solution u_h and can be easily evaluated. The situation is different for the weighting terms ω_K, $\omega_{K,\delta}$ and $\omega_{\partial K}$. Since the system (1)–(4) is too complex for deriving analytically upper bounds for the dual solution z, we need a numerical approximation. This can be done by formulating a 'perturbed' discrete dual problem. Accordingly, we seek $z_h \in X_h$, satisfying the linear system given by the Frechét derivatives $a_h'[u_h]$ of the semi-linear forms a_h previously defined:

$$a_h'[u_h](\phi, z_h) = J(\phi) \quad \forall \phi \in X_h \tag{20}$$

Since this equation is linear, the computational cost of its solution relates to the cost of one Newton step in solving the primal problem. We note that the solution of the dual problem on the same mesh and by the same method as used for the primal problem is not mandatory. One may use a coarser mesh to save computational cost or even employ another (possibly higher-oder) discretization to get the weights with enhanced accuracy. In our computations, the dual solution is always computed by the same method as used for the primal problem.

Having computed an approximation to the exact dual solution z, the weights ω_K given by (20) can be determined in different ways, see [25]. We approximate the weights

Table 10
Nusselt numbers for locally refined meshes obtained by the weighted residual estimator

#dof	η_ω	
	$\langle Nu \rangle_c$	$\|e\|$
4356	−8.74077601	1.190040e−01
5868	−8.838733	2.104700e−02
7980	−8.86380117	4.021166e−03
10964	−8.86567601	5.896010e−03
14660	−8.86133434	1.554339e−03
19268	−8.86864399	8.863992e−03
25708	−8.86612266	6.342663e−03
34148	−8.8629288	3.148805e−03
44828	−8.86428314	4.503139e−03
58748	−8.86427399	4.493989e−03
76508	−8.86365736	3.877358e−03
100188	−8.86254482	2.764818e−03
131052	−8.86168738	1.907378e−03
170436	−8.86073673	9.567350e−04

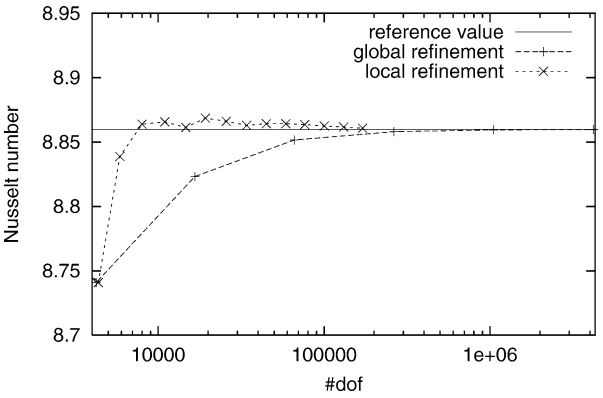

Fig. 5. Convergence of the Nusselt number for tensor meshes and locally refined meshes.

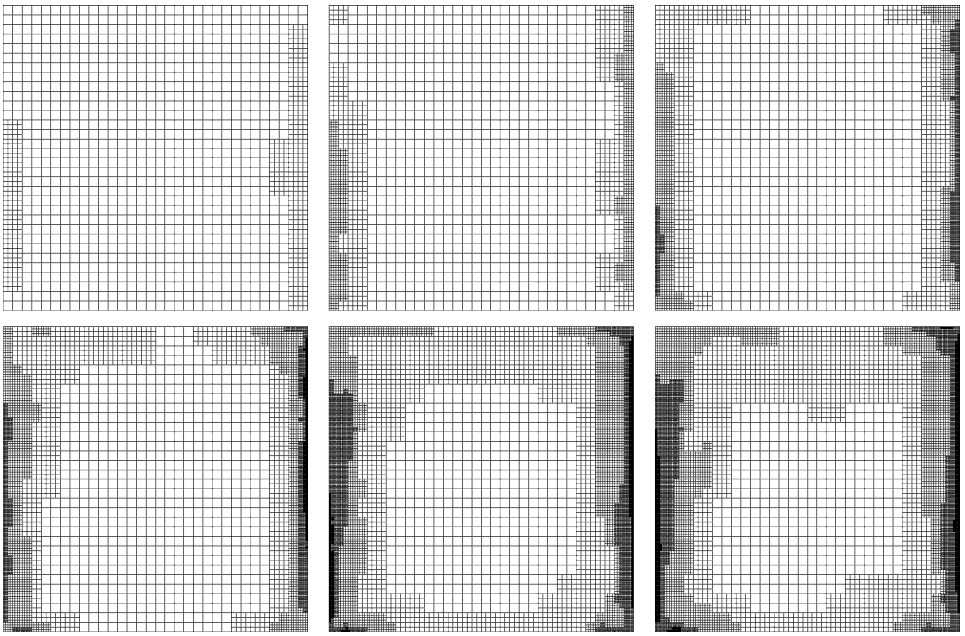

Fig. 6. Locally refined meshes for optimal computation of $\langle Nu\rangle_c$.

by second-order difference quotients of the discrete dual solution $z_h \in V_h$:

$$\omega_K \leqslant Ch_K^2 \left\|\nabla^2 z\right\|_K \approx \widetilde{\omega}_K := Ch_K^3 \left|\nabla_h^2 z_h(x_K)\right| \tag{21}$$

with x_K the center point of K, an interpolation constant $C \sim 0.1$ independent of h_K, where $\nabla^2 z$ is the Hessian of z and $\nabla_h^2 z_h$ a suitable difference approximation. An analogous technique is used in evaluating the two other types of weights $\omega_{\partial K}$ and $\omega_{K,\delta}$ in (19).

Now, we apply local mesh refinement on the basis of this error estimator. In Table 10, we list the obtained Nusselt numbers for Case 1 and the discretization *Discr II*. Comparisons with the previous documented tensor-grid meshes show a substantial improvement, see Fig. 5. For an accuracy of 1%, we need only about 8 000 degrees of freedom, instead of 66 564 on a globally refined mesh (see Table 4). Finally, we show several locally refined meshes in Fig. 6.

References

[1] C.L. Merkle, Y.-H. Choi, The application of preconditioning in viscous flows, J. Comput. Phys. 105 (1993) 207.

[2] H. Bijl, Computation of flow at all speeds with a staggered grid scheme, Master's thesis, Technical University Delft, 1999.

[3] H. Bijl, P. Wesseling, A unified method for computing incompressible compressible flows in boundary-fitted coordinates, J. Comput. Phys. 141 (1998) 153–173.

[4] R.I. Issa, Solution of the implicitly discretised fluid flow equations by operator splitting, J. Comput. Phys. 62 (1985) 40–65.

[5] P.A.B. de Sampaio, M.L. Moreira, A new finite element formulation for both compressible nearly incompressible fluid dynamics, Internat. J. Numer. Methods Fluids 32 (1) (2000) 51–78.

[6] P. Le Quere, H. Paillere, Modelling simulation of natural convection flows with large temperature differences: a benchmark problem for low mach number solvers, announced for publication.

[7] P. Le Quere, Private communication, 2000.

[8] R. Becker, M. Braack, R. Rannacher, Numerical simulation of laminar flames at low mach number with adaptive finite elements, Combust. Theory Modelling 3 (1999) 503–534.

[9] M. Braack, An adaptive finite element method for reactive flow problems, Dissertation, Universität Heidelberg, 1998.

[10] M. Braack, R. Rannacher, Adaptive finite element methods for low-mach-number flows with chemical reactions, in: H. Deconinck (Ed.), 30th Computational Fluid Dynamics, Lecture Series, Vol. 1999-03, von Karman Institute for Fluid Dynamics, 1999, pp. 1–93.

[11] G. de Vahl Davis, I.P. Jones, Natural convection in a square cavity—A comparison exercise, Internat. J. Numer. Methods Fluids 3 (1983) 227–248.

[12] J.G. Heywood, R. Rannacher, S. Turek, Artificial boundaries flux and pressure conditions for the incompressible Navier–Stokes equations, Internat. J. Numer. Math. Fluids 22 (1992) 325–352.

[13] P.G. Ciarlet, Finite Element Methods for Elliptic Problems, North-Holland, Amsterdam, 1978.

[14] C. Johnson, Numerical Solution of Partial Differential Equations by the Finite Element Method, Cambridge University Press, Cambridge, 1987.

[15] V. Girault, P.-A. Raviart, Finite Elements for the Navier–Stokes Equations, Springer, Berlin, 1986.

[16] T.J.R. Hughes, L.P. Franca, M. Balestra, A new finite element formulation for computational fluid dynamics: V. circumvent the Babuska–Brezzi condition: A stable Petrov–Galerkin formulation for the Stokes problem accommodating equal order interpolation, Comput. Methods Appl. Mech. Engrg. 59 (1986) 89–99.

[17] P. Hansbo, A. Szepessy, A velocity-pressure streamline diffusion finite element method for the incompressible Navier–Stokes equations, Comput. Methods Appl. Mech. Engrg. 84 (1990) 175–192.

[18] L.P. Franca, S.L. Frey, Stabilized finite element methods: II. The incompressible Navier–Stokes equations, Comput. Methods Appl. Mech. Engrg. 99 (1992) 209–233.

[19] Y. Saad, Iterative Methods for Sparse Linear Systems, PWS Publishing Company, 1996.

[20] W. Hackbusch, Multi-Grid Methods and Applications, Springer, Berlin, 1985.

[21] R. Becker, M. Braack, Multigrid techniques for finite elements on locally refined meshes, Numer. Linear Algebra Appl. 7 (2000) 363–379, Special Issue.
[22] C.T. Kelley, Iterative Methods for Linear Nonlinear Equations, SIAM, Philadelphia, PA, 1995.
[23] M. Giles, M. Larson, M. Levenstam, E. Süli, Adaptive error control for finite element approximations of the lift drag coefficients in viscous flow, Technical Report NA-76/06, Oxford University Computing Laboratory, 1997.
[24] R. Becker, R. Rannacher, A feed-back approach to error control in finite element methods: Basic analysis examples, East-West J. Numer. Math. 4 (1996) 237–264.
[25] R. Becker, Weighted error estimators for finite element approximations of the incompressible Navier–Stokes equations, Rapport de Recherche RR-3458, INRIA Sophia-Antipolis, 1998.
[26] F.-T. Suttmeier, Adaptive finite element approximation of problems in elasto-plasticity theory, Dissertation, Universität Heidelberg, 1997.